International Journal of Heat and Mass Transfer 52 (2009) 1268–1275

Contents lists available at ScienceDirect

International Journal of Heat and Mass Transfer

journal homepage: www.elsevier.com/locate/ijhmt

Suitability of three different two-equation turbulence models in predicting film cooling performance over a rotating blade

Zhi Tao, Zhenming Zhao, Shuiting Ding, Guoqiang Xu, Hongwei Wu *

National Key Lab. on Aero-Engines, School of Jet Propulsion, Beihang University, Beijing 100083, PR China

ARTICLE INFO

Article history:
Received 17 September 2007
Received in revised form 23 May 2008
Available online 14 November 2008

Keywords:
Turbulence model
Film cooling
Rotating blade
Heat transfer
Experimental

ABSTRACT

The suitability of three different two-equation turbulence models in predicting film cooling effectiveness on a rotating blade was investigated and they are the commonly used standard k-ε model, the k-ω model and the shear stress transport k-ω model. To fulfill this target, both numerical simulation and the experimental investigation were carried out for a rotating blade having a flat test surface with a 4 mm diameter straight circular cooling hole in 30° inclined injection. The blade rotated at five different speeds of 0, 300, 500, 800 and 1000 rpm. The momentum ratio was set to be 0.285 and the Reynolds (Re_D) number based on the mainstream velocity and hydraulic diameter of the mainstream channel is 1.45×10^5. The averaged density ratio was chosen to be 1.026 with air as both the coolant and the mainstream. Comparison between the numerical work and the experimental results indicated that (1) the rotating speed is the most critical parameter influencing the film cooling effectiveness distributions and the pressure surface could be remarkably different from the suction surface, (2) as for the algebraic averaged film cooling effectiveness, numerical predictions of the three turbulence models all overshoot compared with the experimental results, (3) among the three turbulence models, the standard k-ε model gave the poorest prediction.

1. Introduction

Film cooling is widely used to protect gas turbine airfoils from thermal stresses generated by exposure to hot combustion gases and allow for higher turbine inlet temperature. In film cooling, the cooler air bled from the high-pressure compressor is discharged through discrete holes on the turbine blade wall or the end walls and then forms a thin thermal insulation layer to protect the blade surface from being overheated by the hot gas. As a complex interaction between the mainstream and coolant, the cooling performance is known to be affected by a variety of parameters, such as the blade surface curvature, hole arrangement and configuration, injection angle, blowing ratio, Reynolds numbers of the mainstream and the coolant, momentum ratios, mainstream turbulence and rotation number (Rt), etc.

Film cooling has been extensively studied over the past four decades and comprehensive reviews were given by Goldstein [1], Garg and Gaugler [2–4]. In most of film cooling calculations, turbulence models employed in general do not go beyond the isotropic two-equation type [5]. Walters and Leylek [6] performed numerical analyses with the standard k-ε model on a film-cooled flat surface at low freestream turbulence intensity. Their study highlighted that the isotropic turbulence modeling and near-wall treatment was not suitable to capture the jet lift-off and reattachment. They also pointed that the turbulence models that accurately represent anisotropic turbulence will be needed to resolve downstream characteristics, particularly the lateral spreading of the coolant.

Jia et al. [7] published their numerical simulations of the slot film cooling jet with various angles in 2005. Three turbulence models were employed in their study, i.e., the shear stress transport k-ω model (*SST*) of Menter [8], the $k-\varepsilon-\overline{v^2}$ model (V2F) of Durbin [9] and the stress-ω model (RSTM) of Wilcox [10]. For the comparison they used the experimental data with laser Doppler velocimetry (LDV) finished by Chen and Hwang [11] and good agreement between numerical prediction and experimental results was obtained.

Hassan and Yavuzkurt [12] concentrated on the comparison of four different two-equation turbulence models in predicting film cooling performance. The four turbulence models were: the standard k-ε model, the RNG k-ε model, and the realizable k-ε model as well as the standard k-ω model. The capabilities of the four two-equation turbulence models in predicting film cooling effectiveness were investigated and their limitations as well as relative performance were presented. It was concluded that the standard k-ε model has the most promising potential among the two-equation models considered. It was chosen as the best candidate for further improvement for the simulation of film cooling flows.

Turbulence in film cooling is considered as anisotropic, in particular in the region surrounding the film hole and near the wall. Azzi

* Corresponding author. Tel.: +86 (10) 8231 7694; fax: +86 (10) 8231 4545.
E-mail address: hongwei_wu@buaa.edu.cn (H. Wu).

0017-9310/$ - see front matter © 2008 Elsevier Ltd. All rights reserved.
doi:10.1016/j.ijheatmasstransfer.2008.09.008

Nomenclature

D	film hole diameter, mm
C_μ	constant
i	integer variant
k	turbulent kinetic energy, m^2/s^2
n	pixel number
Rt	rotation number ($\Omega D/u_g$)
T	temperature, K
ug	mainstream velocity, m/s
u^*	shear velocity, m/s
x	streamwise coordinate, mm
y	coordinate normal to solid surface, mm
y^+	distance in wall coordinates (yu^*/v)
z	spanwise coordinate, mm

Greek letters

ϵ	turbulent kinetic energy dissipation, m^2/s^3
ρ	density, kg/m^3
η	adiabatic film cooling effectiveness
v	kinetic viscosity, m^2/s
μ	viscosity coefficient, kg/(m s)
ω	turbulence frequency, s^{-1}
Ω	rotational speed, rpm

Subscripts

ad	adiabatic
c	cooling air
g	main flow
t	turbulence
w	wall

and Lakehal [5] compared two classes of turbulence models with respect to their predictive performance in reproducing near-wall flow physics and heat transfer. The study focused on anisotropic eddy-viscosity/diffusivity models and explicit algebraic stress models, up to cubic fragments of strain and vorticity tensors. Their results clearly showed that only the anisotropic eddy-viscosity/diffusivity model could correctly predict the spanwise spreading of the temperature field and reduce the strength of the secondary vortices. In Lakehal's extension work [13], a new modeling strategy using near-wall variation of the turbulent Prandtl number as a function of the local Reynolds number was employed and compared with the results published in Ref. [5]. The comparison between the calculated and measured wall-temperature distributions showed that the anisotropic turbulence model with near-wall variation of the turbulent Prandtl number produced the best agreement.

To the authors' knowledge, however, all the numerical works with both isotropic and anisotropic turbulence models have been carried out for the stationary cases, i.e., the coordinate systems were kept still. The turbine blades are, however, under rotation and extra forces would take part in influencing the film cooling processes and make the phenomena more complicated and make the CFD prediction more difficult. The present paper is the first study of investigating the suitability of turbulence models on predicting film cooling under rotating frames. We carried out the experimental investigation for film cooling over a flat plate under rotation and then we study the performance of commonly-used turbulence models. As the first part of a series of research work, this paper focused on three conventional isotropic turbulence models widely used in engineering, and they are the standard k-ε model, the k-ω model and the shear stress transport k-ω model.

2. Experimental apparatus and measurement procedure

2.1. The rotating test rig

For validation of turbulence models, experimental study was conducted on the rotating heat transfer test rig at the National Key Laboratory on Aero-Engines, Beihang University (Formerly, the Beijing University of Aeronautics and Astronautics), China. The test rig, as shown in Fig. 1, had a 600 mm rotating radius and the rotating speed could be up to 3000 rpm driven by a 30 kW electric motor. The system consisted of the test section, the air supply system and the telemetering data acquisition system. More details of the rotating test rig were described by Tao et al. [14].

2.2. The test model

Fig. 2 shows the schematic drawing of the test model for the current experimental study. The test model was made of bakelite for providing better adiabatic condition, and the material thermal conductivity was $k = 0.28$ W/(m K). The test region was flat with a straight circular film hole in 30° inclined injection located in the middle. The film hole had a diameter of $D = 4$ mm and a length-to-diameter ratio of $L/D = 5.75$. The rotational radius of the film hole was 450 mm. The front section of the test model has a circular shape to simulate the flow over the blade tip and to avoid the main stream separation.

2.3. Temperature measurement

In the present study, the adiabatic film cooling effectiveness (η) was selected as the key parameter in representing the film cooling performance, it was defined as

$$\eta = \frac{T_g - T_{aw}}{T_g - T_c} \tag{1}$$

where, T_g, T_c and T_{aw} are the mainstream temperature, the coolant temperature and the adiabatic wall temperature, respectively.

In the experiment, two T-type (copper-constantan) thermocouples were installed upstream of the test models to measure the mainstream temperatures and one T-type thermocouple was located in the coolant chamber to measure the coolant temperatures.

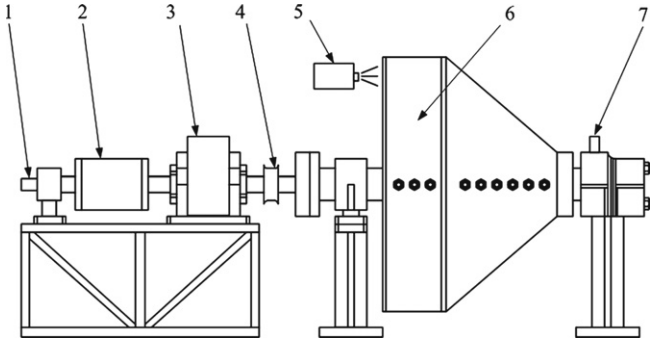

1 Coolant inlet, 2 Telemetering instrument, 3 Carbon brush-copper collar, 4 Conveyor, 5 Digital camera, 6 Test section, 7 Hot air inlet

Fig. 1. Schematic diagram of the experimental rig.

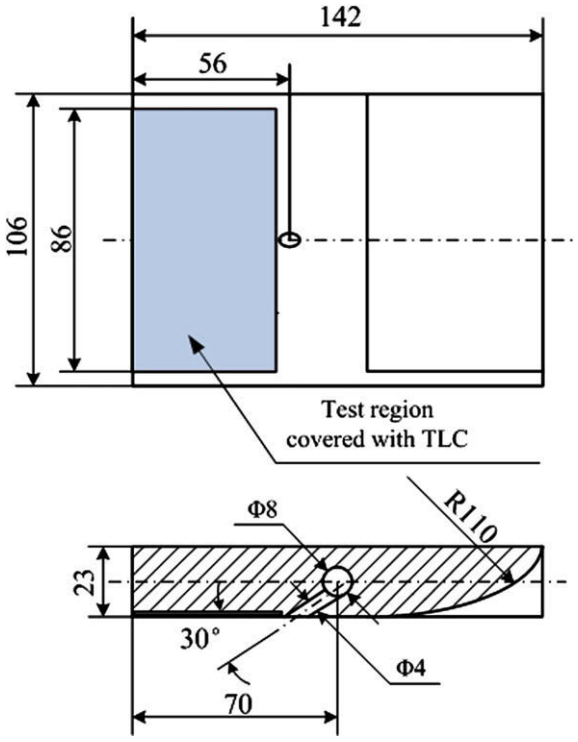

Fig. 2. Side and cutaway view diagram of the test section.

All these temperature signals were transferred to the computer via the telemetering instrument.

In order to obtain the test surface temperature distributions, the thermochromic liquid crystal (TLC) technique was employed. Numerous studies using liquid crystal thermography have been described in the open literatures (Baughn [15], Camci et al. [16], Chyu et al. [17], Newton [18], Owen [19]), and will not be repeated here. For the image acquisition, a high resolution (7.1 million pixels) digital camera (Canon PowerShot G6) was mounted aside the test rig to capture the TLC images, as shown in Fig. 1.

To reveal the relationship between the hue values of the TLC image and the temperatures, a prior calibration experiment was implemented and a fitted polynomial calibration curve to the power of 10 was obtained, as shown in Figs. 3 and 4.

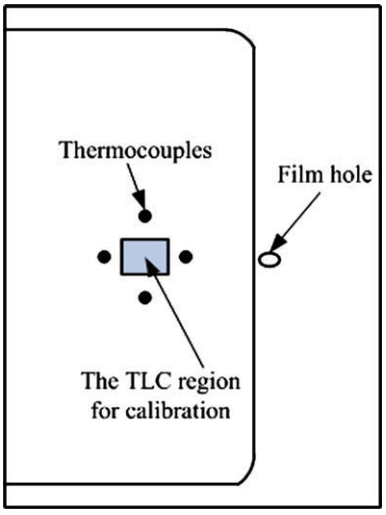

Fig. 3. Thermocouple arrangements for the liquid crystal calibration.

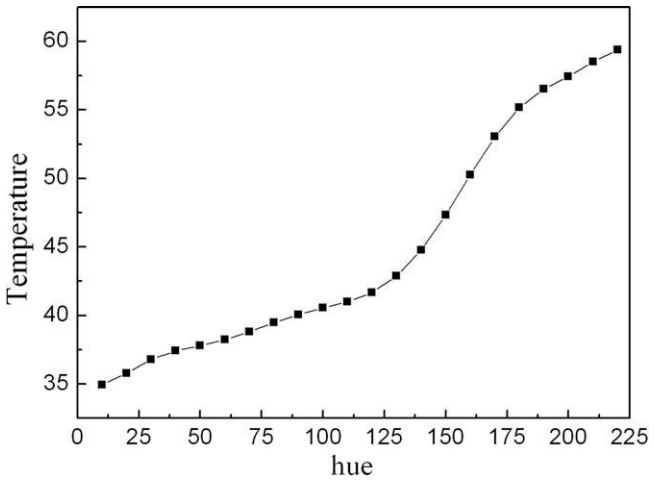

Fig. 4. Calibration curve for liquid crystal.

2.4. Operating conditions

During the test, the only variable parameter was the rotating speed and all the rest were kept constant. There were five different rotating speeds and they were: 0, 300, 500, 800 and 1000 rpm. The momentum ratio was fixed at a constant of 0.285. The Reynolds number based on the mainstream velocity and hydraulic diameter of the mainstream channel was 1.45×10^5. The density ratio was equal to 1.026 and the temperature ratio was kept constant at 0.968.

2.5. Uncertainty of the adiabatic film effectiveness measurement

Following the error transfer function, the uncertainty of adiabatic film effectiveness could be calculated as:

$$\Delta\eta_{ad}=\sqrt{\left[\frac{T_{aw}-T_c}{(T_g-T_c)^2}\right]^2(\Delta T_g)^2+\left(\frac{1}{T_g-T_c}\right)^2(\Delta T_{aw})^2+\left[\frac{T_g-T_{aw}}{(T_g-T_c)^2}\right]^2(\Delta T_c)^2} \quad (2)$$

Based upon the fluctuation of the temperature signal, the uncertainty of T_c and T_g was within ±0.5 K. The uncertainty of the liquid crystal was below ±0.1 K. Therefore, for the current experimental data at Ω = 1000 r/min, T_c = 309.4 K, T_g = 319 K, T_{aw} = 314.2 K, the uncertainty of the experimental adiabatic effectiveness is 7.6%.

3. Computational details

Fig. 5 illustrates the coordinate system in the present experimental and numerical studies. The *x*-axis is along the mainstream direction, *y*-axis is normal to the test surface and the *z*-axis conforms to the right-hand law. The origin is located at the downstream tip of the film hole.

Following this reference frame, four key areas, namely, the computational model, the mesh, the boundary conditions, the solution method and more important the turbulence models themselves are addressed below.

3.1. Computational model and mesh

For comparison, the CFD study chose the same geometry of the experimental work outlined above as the computational domain. Since an adiabatic wall boundary was adopted for the test surface, the computational model only included the flow domain as shown in Fig. 6.

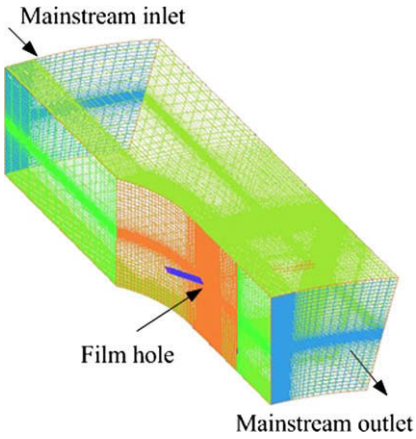

Fig. 5. Illustration of the computational domain.

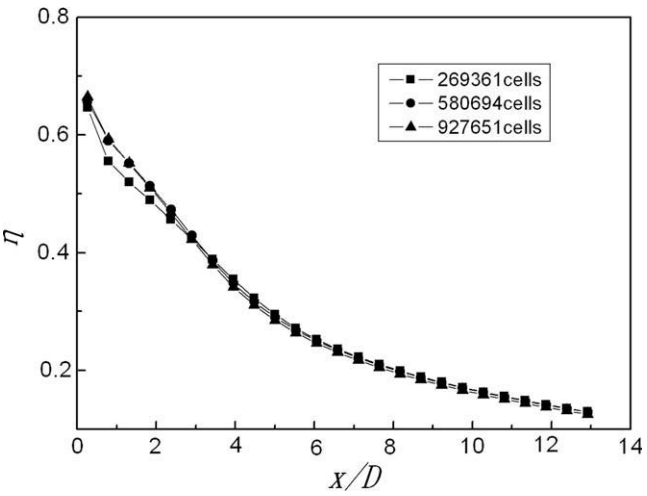

Fig. 6. Comparisons of numerical results with different grids.

Fig. 6 also shows the mesh used and it was made up of object-based, multi-block and structured hexahedral grids. Prior to the actual numerical simulation, a grid independence study was performed by using different grids with 269,361, 580,694 and 927,651 cells, respectively. As shown in Fig. 7, the predicted film cooling effectiveness changed by less than 0.7% as the grid increased from 580,694 to 927,651 cells, while a maximum of 8.3% was observed as the grid increased from 269,361 to 580,694. Therefore, a compromise between computation accuracy and computing capability led to the use of 580,694 cells. There were 148 cells in the mainstream direction, 60 in the spanwise direction and 60 in the normal direction to the wall surface. In the computational domain, the o-grids were applied inside the film hole to improve mesh quantity. Noted that the first grid point adjacent to all the bounding wall surfaces was spaced within a y^+ of 2 in order to meet the requirements for the two-layer near-wall treatment.

3.2. Boundary conditions

To comply with the experiments, following boundary conditions were employed:

- Mass flow rate: 0.2 kg/s for mainstream, and 1.906×10^{-4} kg/s for coolant to maintain a constant mainstream Reynolds number at 1.45×10^5 and the momentum ratio at 0.285.

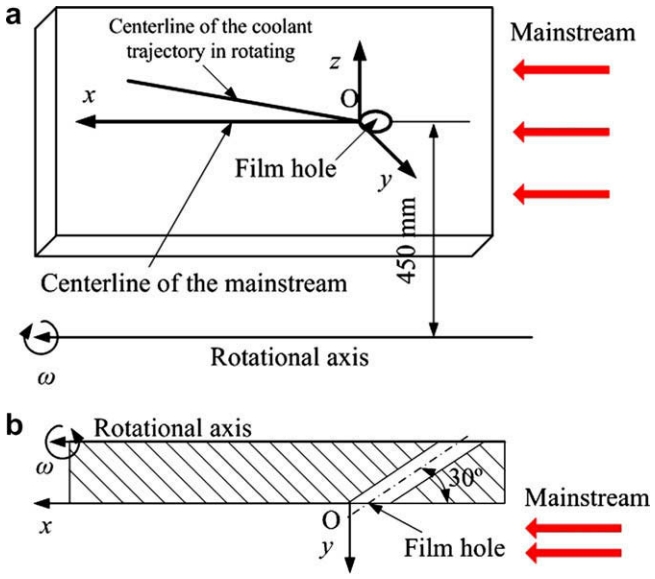

Fig. 7. Coordinates system.

- Temperature: 321.15 K for mainstream, and 311.15 K for coolant to keep the temperature ratio at 0.968.
- Turbulence intensity: this parameter was not measured during the experiment and a honeycomb was however installed before the test section to regulate the mean flow and reduce the turbulence. A 5% turbulence intensity was assumed for both mainstream and coolant for CFD simulation.
- Wall surfaces: no slip and adiabatic boundary condition.
- Outlet: constant pressure at 1 atm.

3.3. Turbulence models

The aim of this paper was to select the best candidate for film cooling prediction among the mostly used two-equation turbulent models. Two-equation turbulence models are taken to be the most basic of the 'complete' turbulence models in which the transport equations of the turbulent kinetic (k) and its dissipation rate (ε) are used independently to simulate the velocity field and capture flows affected by variable length scales. In the present study, the three turbulent models we chose were the standard k-ε model, the k-ω model and the *SST* k-ω turbulence model.

The k-ε and k-ω two-equation models use the gradient diffusion hypothesis to relate the Reynolds stresses to the mean velocity gradients and the turbulent viscosity. The turbulent viscosity is modeled as the product of a turbulent velocity and turbulent length scale.

The k-ε model, like the zero equation model, is based on the eddy viscosity concept, so that

$$\mu_{\text{eff}} = \mu + \mu_{\text{t}} \tag{3}$$

where μ_{t} is the turbulence viscosity. The k-ε model assumes that the turbulence viscosity is linked to the turbulence kinetic energy and dissipation via the relation

$$\mu_{\text{t}} = C_{\mu}\rho\frac{k^2}{\varepsilon} \tag{4}$$

where C_{μ} is the k-ε turbulence model constant which is equal to 0.09 in the current study.

The k-ω models assumes that the turbulence viscosity is linked to the turbulence kinetic energy and turbulent frequency via the relation

$$\mu_t = \rho \frac{k}{\omega} \tag{5}$$

where ω is the turbulence frequency.

One of the advantages of the k-ω formulation is the near-wall treatment for low-Reynolds number computations. This model does not involve the complex non-linear damping functions required for the k-ε model.

The k-ω-based *SST* model used in current study is the same as Menter's [20] which accounts for the transport of the turbulent shear stress. The modifications include the addition of a cross-diffusion term in the ω equation and a blending function to ensure that the model equations behave appropriately in both the near-wall and far-field zones (Jia et al. [7]).

3.4. Solution method

All simulations for the present work were solved with the STAR-CD commercial software and run on a cluster of 16 parallel 2.4 GHz processors with a memory of 16,384 MB. Calculations were performed with the bounded second-order upwind biased discretization. All solutions were converged to 1×10^{-5} and grid-independence was established. A single iteration took approximately 24 s, and generally about 800 iterations were required for convergence for each case.

4. Results and discussion

4.1. Averaged film cooling effectiveness

In the current study, the algebraic averaged film cooling effectiveness was evaluated for a limited region of $3D \times 3D$ downstream the film exit as shown in Fig. 8. The averaged effectiveness was defined as:

$$\overline{\eta_{ad}} = \frac{\sum_{i=1}^{n} \eta_{ad,i}}{n} \tag{6}$$

where n is the number of pixels in a given area.

Fig. 9 is the averaged film cooling effectiveness $\overline{\eta_{ad}}$ versus five different rotating speeds from 0 to 1000 rpm. On the pressure surface, the measured $\overline{\eta_{ad}}$ increases sharply with Ω increasing from stationary up to 500 rpm, and then begins to decrease when the rotating speed goes higher. As a result, an evident peak value around 500 rpm can be clearly found. However, the CFD predictions with the three chosen turbulent models were not satisfactory and they all failed in revealing this tendency of variation. The k-ε model predicted monotone decreasing and the other two, on the contrary, were monotone increasing. At stationary, the k-ε model overshoots by 17.6% compared with the experimental result and the other two models underestimated by 8.7% for *SST* and 6.4% for the k-ω model. At the highest rotating speed of 1000 rpm, the k-ε model overshot by 7.1% and the other two models underestimated by 6.5% for *SST* and 9.1% for the k-ω model. The maximum deviations were 27.8% for the k-ω model and 27% for the *SST* and they all took place at 500 rpm, while the k-ε model deviated most by 17.6% at stationary. Deviations of turbulence models from the experimental results may be due to the highly anisotropic nature of the turbulence [21].

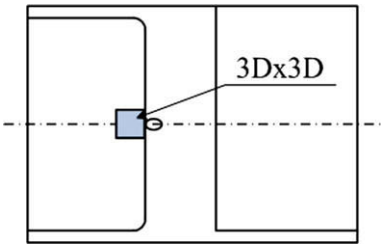

Fig. 8. Sketch map of algebraic averaged area downstream the film hole.

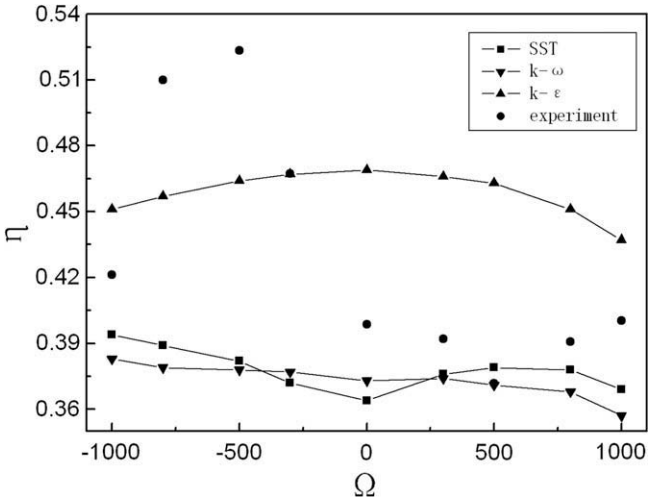

Fig. 9. Average film cooling effectiveness profiles downstream the film hole.

On the suction surface, the measured $\overline{\eta_{ad}}$ first decreased and then began to increase with the rotating speed going up and the minimum value occurred at around 500 rpm. However, the predictions were still not satisfactory compared with the experimental results and failed in predicting the tendency of $\overline{\eta_{ad}}$ versus the rotating speeds. The standard k-ε and k-ω models showed monotone decreasing while the *SST* k-ω turbulence model was opposite. At 1000 rpm, the k-ε model overpredicted by 9.1% and the other two models underestimated by 7.8% for *SST* and 10.8% for the k-ω model. The maximum deviation by 24.5% was found at 500 rpm for the k-ε model, and on the contrary, the minimum deviations by 1.9% for *SST* and 0.2% for the k-ω model were observed at Ω = 500 rpm.

4.2. Film cooling effectiveness along the centerline downstream the film hole

Fig. 10 presents the profiles of experimental and numerical adiabatic film cooling effectiveness along the center line downstream the film hole with five different rotating speeds, i.e., 0, 300, 500, 800 and 1000 rpm. Again, obvious discrepancies existed between CFD simulations and their experimental counterparts.

Experimental results showed that rotation led to increase in cooling effectiveness and especially for the region near the hole. This increase was maximized when rotating speed reached 500 rpm and it enjoyed a 45.5% augmentation. When rotating speed was even higher, this augmentation was weakened and was merely 6.9% for 1000 rpm. For both the pressure side and the suction side, we have seen that the cooling effectiveness was monotone decreasing along the centerline and the variations were all concave curves.

As for the CFD simulation, the standard k-ε model was the worst among the three and, with it, the cooling effectiveness was almost unchanged and remained almost 1.0 for the region near the hole with $x/D < 1$ for both the pressure side and the suction side. Predictions by the standard k-ε model were all convex curves.

The k-ω and *SST* k-ω turbulence models were relatively better and the two behaved almost the same too. The two models predicted a sharp decrease in cooling effectiveness near the hole with $x/D < 0.2$, which was close to the experimental phenomena. After this fast falling region, the film cooling effectiveness began to drop

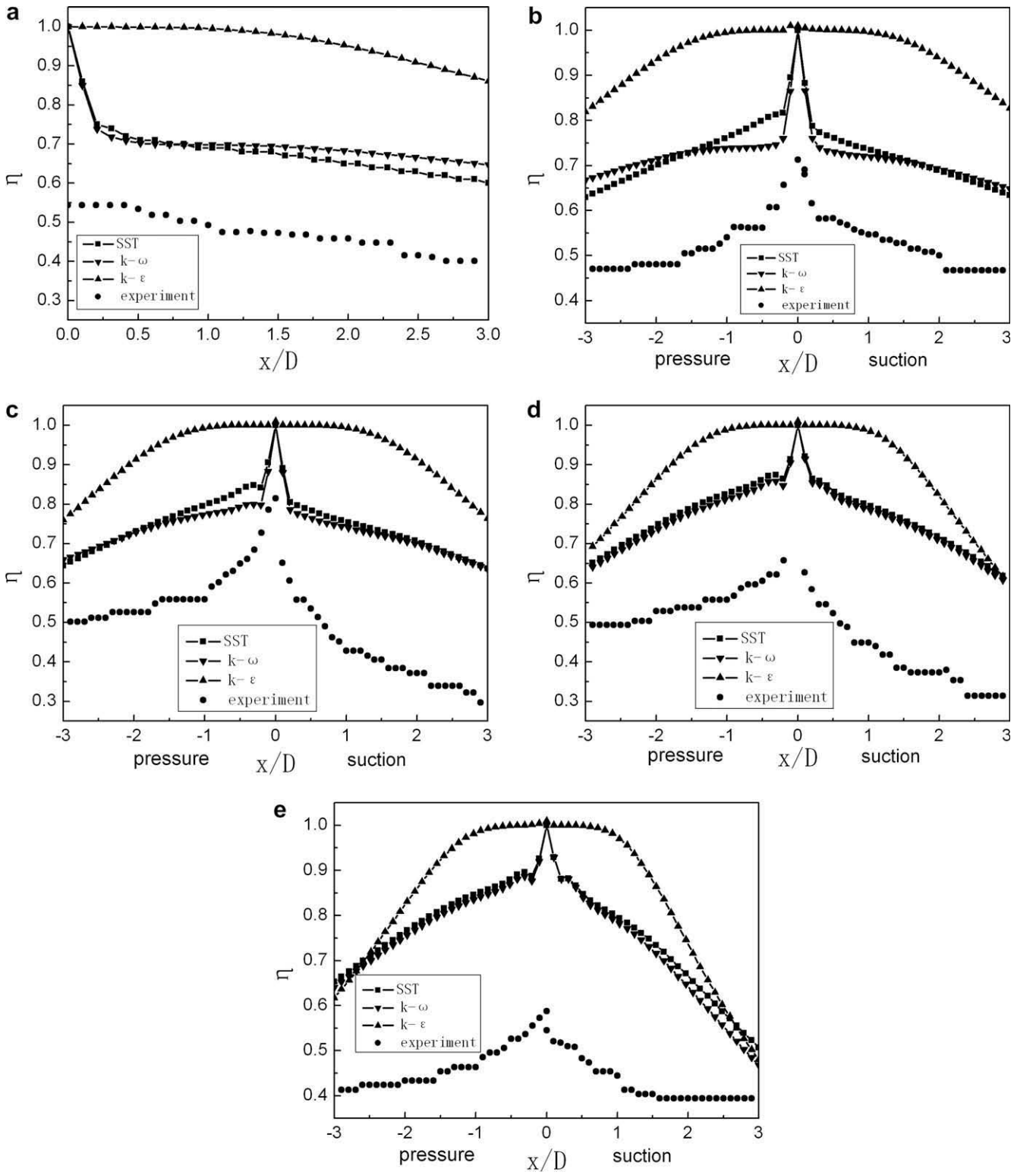

Fig. 10. Film cooling effectiveness along the center line downstream the film hole. (a) Stationary; (b) 300 rpm; (c) 500 rpm; (d) 800 rpm; (e) 1000 rpm.

gradually. For most of the cases, the two models nearly coincided and the greatest discrepancy took place for the region right after the fast falling region until *x/D* was around 1.0 and this discrepancy vanished when rotating speed was over 500 rpm. Though the *k-ω* and *SST k-ω* turbulence models were relatively better in accuracy, they still displayed great disagreement with the experimental results.

The reason for the obvious discrepancy between CFD simulation and the experimental work may be because of the anisotropy of the film cooling flow field. Many researchers [22] [23] have shown that the turbulence mixing between the jet and mainstream is three dimensional and a pair of counter-rotating vortices occurs downstream the film hole due to the disturbance of coolant injection. As a result, the flow field of film cooling is

quite complicated and anisotropic. Furthermore, in the rotating cases, the action of Coriolis and buoyancy force not only alter the movement of the main flow but generate strong secondary flow as well and this makes the flow field even complicated and the counter-rotating vortices asymmetric. The three turbulent models we chose, however, are all with the assumption of isotropy.

4.3. Film cooling effectiveness along the centerline of coolant trajectory

Compared with the stationary coordinating system, fluid under rotating frame is influenced by two additional forces, the Coriolis force and the centrifugal force. Under these forces, apart from the heavy secondary flow induced, the coolant was expected to yaw from the pervious trajectory. Therefore, it is interesting to

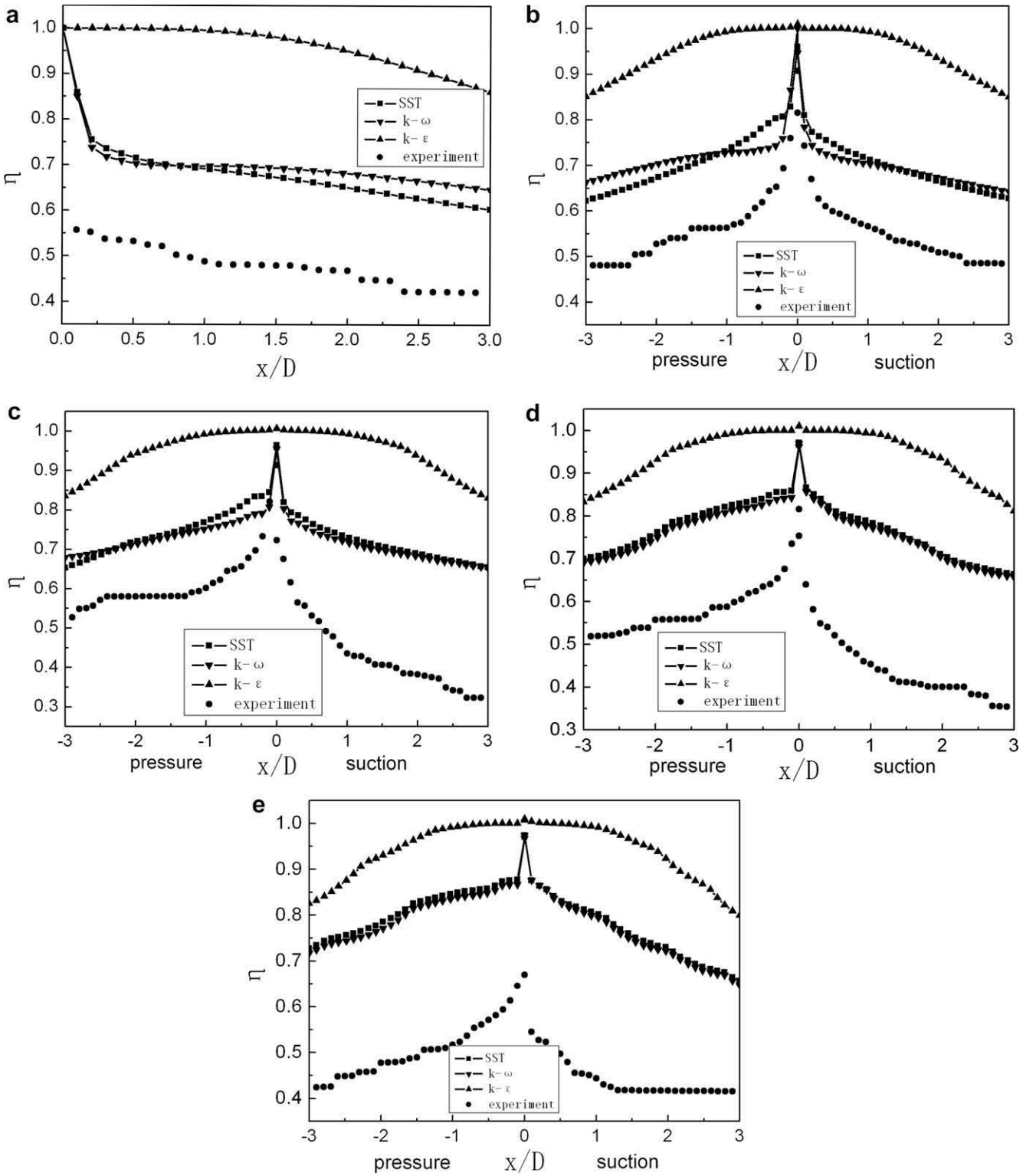

Fig. 11. Film cooling effectiveness along the coolant trajectory downstream the film hole. (a) Stationary; (b) 300 rpm; (c) 500 rpm; (d) 800 rpm; (e) 1000 rpm.

do the comparison again along the centerline of coolant actual trajectory instead of the geometric centerline. The corresponding results were shown in Fig. 11(a)∼(e) and significant discrepancies were also obvious between the CFD simulations and their experimental counterparts.

From the experimental results, we could see that the η_{ad} along the trajectory were quite similar in shape to the corresponding results along the geometric centerline as shown in Fig. 10 and the differences, however, were rather on the magnitude. For the region of $x/D < 0.3$, the measured cooling effectiveness along the film trajectory was higher than that along the centerline and the maximum discrepancy could be as high as 33.3% at the speed of 800 rpm.

As for the CFD simulation, the standard k-ε model again performed the worst among the three compared with the experimental results while the k-ω and *SST* k-ω turbulence models were relatively better. Along the film trajectory, in the region of $x/D < 1$, the film cooling effectiveness of standard k-ε model still remained about 1.0 and then monotone decrease with the increase of x/D. This leads to a large difference to the experimental data and the maximum deviation of 60% can be found at the speed of 1000 rpm.

The k-ω and *SST* k-ω turbulence models performed almost the same effect on the modeling and represented better agreement in trend than the standard k-ε model compared with the measurement. However, they still displayed great overpredictions to the experimental results. The maximum deviation is about 44.9% at $\Omega = 1000$ rpm.

This deviation between the CFD and experiment may be attributed to the isotropic characteristics of the turbulence models as explained in Section 4.2.

5. Conclusions

An experimental and numerical study has been carried out to investigate the suitability of three commonly used turbulence models for the film cooling prediction under rotating frames. A flat test section with a straight circular hole in 30° inclined injection was used and the thermochromic liquid crystal technique was employed for temperature measurement. Three two-equation turbulence models, i.e., the standard k-ε model, the k-ω model and the shear stress transport k-ω turbulence model, were examined and compared with the experimental data. Major findings of this study are as follows:

1. Rotating speed is an important parameter influencing the film cooling effectiveness distributions. On the pressure surface, with the increase of rotating speed, the $\overline{\eta_{ad}}$ first increased to a peak value and then began to decrease. Our test indicated that the maximum value took place at $\Omega = 500$ rpm. On the suction surface, however, the variations of $\overline{\eta_{ad}}$ were opposite and the minimum value was also taking place at the speed of 500 rpm.
2. For the $\overline{\eta_{ad}}$ prediction under rotation, the standard k-ε model was the worst in performance and the k-ω and *SST* k-ω turbulence models were relatively better and produced closer estimation for both the suction surface and the pressure surface. We have to say, however, that all the three turbulence models chosen were not capable in giving reasonable $\overline{\eta_{ad}}$ estimations and this may be due to their isotropic characteristics and further work may have to be carried out in the direction of anisotropic turbulence models.

Acknowledgements

The financial support from the program of New Century Excellent Talents in Beihang University (Grant No. Ncet-05-0189), and partly from the Fanzhou Youth Science Foundation (20070401) is greatly acknowledged. Assistances from people for this study are also greatly appreciated.

References

[1] R.J. Goldstein, Film Cooling, Advances in Heat Transfer, vol. 7, Academic Press, New York, 1971. pp. 321–379.
[2] V.K. Garg, R.E. Gaugler, Heat transfer in film-cooled turbine blades, ASME Paper 93-GT-81 (1993).
[3] V.K. Garg, R. E. Gaugler, Prediction of film cooling on gas turbine airfoils, ASME Paper 94-GT-16 (1994).
[4] V.K. Garg, R.E. Gaugler, Leading edge film cooling effects on turbine blade heat transfer, Numer. Heat Transfer A 30 (1996) 165–187.
[5] A. Azzi, D. Lakehal, Perspectives in modeling film cooling of turbine blades by transcending conventional two-equation turbulence models, Int. J. Turbomach. 124 (2002) 472–484.
[6] D.K. Walters, J.H. Leylek, A systematic computational methodology applied to a three-dimensional film cooling flowfield, ASME J. Turbomach. 119 (1997) 777–785.
[7] R.G. Jia, B. Sunden, P. Miron, B. Leger, A numerical and experimental investigation of the slot film-cooling jet with various angles, ASME J. Turbomach. 127 (2005) 635–645.
[8] F.R. Menter, Two-equation eddy-viscosity turbulence models for engineering applications, AIAA J. 32 (1) (1994) 85–104.
[9] P.A. Durbin, Separated flow components with $k-\varepsilon-\overline{v^2}$ model, AIAA J. 33 (4) (1995) 659–664.
[10] D.C. Wilcox, Turbulence Modeling for CFD, DCW Industries Inc., La Canada, CA, 1998.
[11] K.S. Chen, J.Y. Hwang, Experimental study on the mixing of one-and Dual-line heated jets with a cold crossflow in a confined channel, AIAA J. 29 (3) (1991) 353–360.
[12] J.S. Hassan, S. Yavuzkurt, Comparison of four different two-equation models of turbulence in predicting film cooling performance, ASME Turbo Expo: Power for Land, Sea and Air, GT2006-90860 (2006).
[13] D. Lakehal, Near-wall modeling of turbulent convective heat transport in film cooling of turbine blades with the aid of direct numerical simulation data, Int. J. Turbomach. 124 (2002) 485–498.
[14] Z. Tao, X.J. Yang, S.T. Ding, G.Q. Xu, H.W. Wu, H.W. Deng, X. Luo, Experimental study of rotation effect on film cooling over the flat wall with a single hole, Exp. Thermal Fluid Sci. 32 (2008) 1081–1089.
[15] J.W. Baughn, Liquid crystal methods for studying turbulent heat transfer, Int. J. Heat Fluid Flow 16 (1995) 365–375.
[16] C. Camci, B. Glezer, J.M. Owen, R.G. Pilbrow, B.J. Syson, Application of thermochromic liquid crystal to rotating surfaces, ASME J. Turbomach. 120 (1998) 100–103.
[17] M.K. Chyu, H. Ding, J.P. Downs, F.O. Soechting, Determination of local heat transfer coefficient based on bulk mean temperature using a transient liquid crystals technique, Exp. Thermal Fluid Sci. 18 (1998) 142–149.
[18] P.J. Newton, Y.Y. Yan, N.E. Stevens, S.T. Evatt, G.D. Lock, J.M. Owen, Transient heat transfer measurements using thermochromic liquid crystal Part 1: An improved technique, Int. J. Heat Fluid Flow 24 (2003) 14–22.
[19] J.M. Owen, P.J. Newton, G.D. Lock, Transient heat transfer measurements using thermochromic liquid crystal Part 2: Experimental uncertainties, Int. J. Heat Fluid Flow 24 (2003) 23–28.
[20] F.R. Menter, A comparison of some recent eddy-viscosity turbulence models, J. Fluids Eng. 118 (1996) 514–519.
[21] Y.L. Lin, T.I.P. Shih, Film cooling over flat convex and concave surfaces, AIAA-99-0344 (1999).
[22] M. Tyagi, S. Acharya, Large eddy simulation of film cooling flow from an inclined cylindrical jet, ASME J. Turbomach. 125 (2003) 734–742.
[23] F. Yuan, X.C. Zhu, Z.H. Du, Experimental investigation for the effect of rotation on three-dimensional flow field in film-cooled turbine, Chin. J. Mech. Eng. 20 (1) (2007) 10–15.